Front. Earth Sci. 2023, 17(1): 293−309
https://doi.org/10.1007/s11707-022-1045-7

RESEARCH ARTICLE

Gas-in-place and its influence factors of the upper Paleozoic coal-bearing shale in the Qinshui Basin, China

Chengang LU[1], Ping GAO (✉)[1], Gang LI[1], Yue FENG[1], Xiaorong QU[2], Yufei SU[2], Xianming XIAO[1]

1 School of Energy Resources, China University of Geosciences (Beijing), Beijing 100083, China
2 Shanxi Coal Geology Surveys Research Institute, Taiyuan 030031, China

Abstract Coal-bearing shale shows great potential for unconventional gas resources in China, while its exploration and development have been challenging for a long time. Gas-in-place (GIP) is critical to shale gas evaluation, but the major factors controlling the GIP content of coal-bearing shale remain unclear. To address this issue, the coal-bearing shales of the upper Carboniferous-lower Permian Taiyuan and Shanxi formations in the Zuoquan Block, Qinshui Basin, China, were collected for GIP measurements and an integrated investigation, including organic geochemistry, inorganic mineral compositions, and pore characterizations, was carried out. Our results show that the GIP content of the studied shales displays relatively low values and wide variations, which range from 0.30 to 2.28 m^3/t. The GIP is dominated by desorbed gas and residual gas. Total organic carbon (TOC) contents of the studied shales vary from 0.92% to 16.91%, and inorganic minerals are dominated by clays that mainly consist of illite/smectite mixed layer (I/S) and kaolinite. Inorganic pores have been widely observed in the studied shales, while the organic matter-hosted pores are rarely found using SEM observations. Total porosity of the studied shales is primarily contributed by clay minerals, followed by organic matter and quartz. Weak positive relationships between the GIP content and pore structure parameters imply that the adsorption of methane to nanopores is relatively weak, which may be attributed to the hydrophilicity of clay-hosted pores. Moreover, hydrophobic organic pores are not well developed. Positive correlations between the GIP contents and contents of TOC, clays, and the I/S indicate that major factors influencing the GIP contents of the coal-bearing shales are clays (especially I/S) and TOC content. In summary, these findings would be very helpful to reveal the enrichment mechanism of coal-bearing shale gas and provide a scientific basis for the exploration and development of coal-bearing shale gas.

Keywords coal-bearing shale, clay minerals, inorganic pore, gas potential, unconventional gas

Received December 30, 2021; accepted August 31, 2022

E-mail: gaoping1212@cugb.edu.cn

1 Introduction

Marine shale gas has been commercially produced in the United States and China (Jarvie et al., 2007; Pollastro 2007; Guo and Zhang, 2014; Dong et al., 2015; Zhao et al., 2020), and marine-continental transitional shale gas has also received increasing attention in recent years (Liu et al., 2018; Xi et al., 2018; Cortes et al., 2019; Chen et al., 2020a; Li et al., 2021a; Zhang et al., 2021). Previous works have shown that marine-continental transitional shale has great potential for gas resources in China, and the estimated geological reserves have proven to be approximately 19.8×10^{12} m^3, accounting for 25% of the total shale gas reserves in China (Kuang et al., 2020). Marine-continental transitional deposits are mostly composed of coal measures (Peng et al., 2019), which are also intercalated with organic-rich shales, i.e., so-called "coal-bearing shale" (Peng et al., 2019; Liang et al., 2020a).

Gas-in-place (GIP) is an important parameter for shale gas evaluation (Ross and Bustin, 2008; Li et al., 2022). Few authors have reported that the GIP content of Permian coal-bearing shales vary from 0.35 to 6.43 m^3/t (Tang et al., 2016; Guo et al., 2018; Jia et al., 2020; Shao et al., 2021), which are generally lower than that of marine shales (Dong et al., 2015; Zhao et al., 2016). The factors controlling the GIP content of shales have been extensively studied (Chalmers and Bustin, 2007; Ross and Bustin, 2008; Zhang et al., 2012; Gasparik et al., 2014; Saidian et al., 2016), and mainly include shale compositions and geological conditions. The former include the total organic carbon (TOC) content, thermal

maturity, kerogen type, inorganic mineral compositions, porosity, and pore structure. The latter include moisture, temperature, pressure, and preservation conditions. As for wells within the same block or adjacent to each other, they have similar geological conditions. Hence, it is widely accepted that the GIP content of marine shales is mainly controlled by TOC contents; with increasing TOC contents, the porosity and specific surface area of shales increase, which provide more storage space and adsorption sites for methane, thus leading to high GIP contents (Ross and Bustin, 2008; Zhang et al., 2015; Sun et al., 2020a; Li et al., 2021b). However, the TOC content of coal-bearing shales is comparable with or higher than that of marine shales, and the GIP content of the former is lower than that of the latter. Thus, the major factors influencing the GIP content of coal-bearing shales still remain controversial. Some authors have suggested that the TOC content is still the major factor controlling the GIP content of coal-bearing shales (Li et al., 2020a). However, many authors have found that the adsorbed gas content of coal-bearing shales is controlled by clay contents rather than TOC contents due to the presence of a significant positive correlation between adsorbed gas and clay contents (Zhang et al., 2019a; Qiao et al., 2020). Therefore, it is necessary to study the compositional differences between marine shales and coal-bearing shale and their potential influences on the gas contents.

Coal-bearing shales show different characteristics of organic matter (OM) and inorganic mineral compositions relative to marine shale. In general, marine shales have oil-prone kerogen (type I-II) showing great hydrocarbon generation potential, while coal-bearing shales are gas-prone source rocks (i.e., type III kerogen) (Vandenbroucke and Largeau, 2007; Peng et al., 2019; Sun et al., 2020b). The mineral composition of the Chinese coal-bearing shales mainly includes clay minerals (average = 30%−70%) (Zhang et al., 2017a; Zhang et al., 2018; Tang et al., 2020; Xie et al., 2021; Li et al., 2021a), whereas that of marine shales is dominated by quartz and other brittle minerals (generally > 50%) (Chen et al., 2020b; Wang et al., 2020a). In particular, high-quality gas shale reservoirs have clay contents less than 20% (Qin et al., 2010). In addition to the total clay contents, the relative contents of different clay species in coal-bearing shale and marine shale are different. For example, the clay species of marine shales are dominated by illite, while coal-bearing shales are characterized by high contents of kaolinite and illite/smectite mixed layers (I/S) (Zhang et al., 2019b). The obvious differences in the GIP contents between coal-bearing shale and marine shale may be controlled by these internal factors. Nevertheless, the major factors influencing the GIP contents of coal-bearing shales still need to be further clarified.

In the Qinshui Basin of north China, the upper Carboniferous–lower Permian Taiyuan and Shanxi formations are mainly composed of coal and coal-bearing deposits; coal seams and organic-rich coal-bearing shales are widely developed, and the resources of coalbed methane (CBM) and coal-bearing shale gas are proven to be abundant, with predicted resources of 5.39×10^{12} m^3 and 2.14×10^{12} m^3, respectively (Su et al., 2016). The CBM has been commercially exploited in the Qinshui Basin for a long time (Zou et al., 2018; Yu et al., 2020; Zhu and Salmachi, 2021), but the progress of shale gas exploration and development is slow (Li et al., 2018a; Xi et al., 2018; Yin and Guo, 2019; Zhang et al., 2019b; Liang et al., 2020a; Zhang et al., 2020). Extensive exploration activities have revealed that coal-bearing shales generally have low and varied GIP contents (Zhang et al., 2019a; Zhang and Fu, 2019; Li et al., 2020a). To exactly locate the 'sweet-spot', it is very urgent to explore the major factors that influence the GIP contents of the coal-bearing shales.

In this study, an integrated investigation of the coal-bearing shales from two wells in the Zuoquan Block in the eastern Qinshui Basin, including organic geochemistry, inorganic mineral compositions, pore characterizations, desorption tests and GIP evaluation, was conducted to explore the major factors that influence the GIP contents, thus providing a scientific basis for the further exploration and development of coal-bearing shale gas in the Qinshui Basin and other basins.

2 Samples and analytical methods

2.1 Samples

The Qinshui Basin, with a total area of 3×10^4 km^2, is located in Shanxi Province of north China, and the basin contains a sedimentary succession of the Cambrian, Ordovician, Pennsylvanian, Permian, Triassic, Jurassic, Neogene, and Quaternary (Peng et al., 2017). The upper Carboniferous–lower Permian Taiyuan and Shanxi formations have received a succession of coal and coal-bearing deposits formed in the marine-continental transitional facies (Zhang et al., 2017b; Li et al., 2018b). Organic-rich coal-bearing shales are usually associated with coal seams, which are the primary target for shale gas exploration (Li et al., 2018a). The Taiyuan Formation, with a total thicknesses of 76−177 m, is mainly composed of shale, fine-grained sandstone, limestone, and coal seams. The Shanxi Formation has total thicknesses of 35−72 m, which chiefly consists of fine-grained sandstone, shale, and coal (Shao et al., 2007). The cumulative thicknesses of organic-rich coal-bearing shales vary from 40 to 120 m in both formations (Zhong et al., 2020).

The Zuoquan Block located in the eastern Qinshui Basin is our study area, where the Taiyuan and Shanxi formations, with burial depths of 1400−1800 m, are

favorable targets for shale gas exploration (Xi et al., 2017b; Zhao et al., 2019). A total of 15 coal-bearing shale samples were collected from the Wells 1-1 and 3-2 in the Zuoquan Block (Fig. 1). Detailed information of the studied samples is provided in Table 1. All samples were prepared for geochemical and mineralogical analyses by grinding to a 200 mesh size.

2.2 Analytical methods

2.2.1 *In situ* gas desorption and calculation of the GIP content

The *in situ* gas desorption of fresh core samples was conducted, and the detailed principle and analytical processes were described by previous authors (Deng

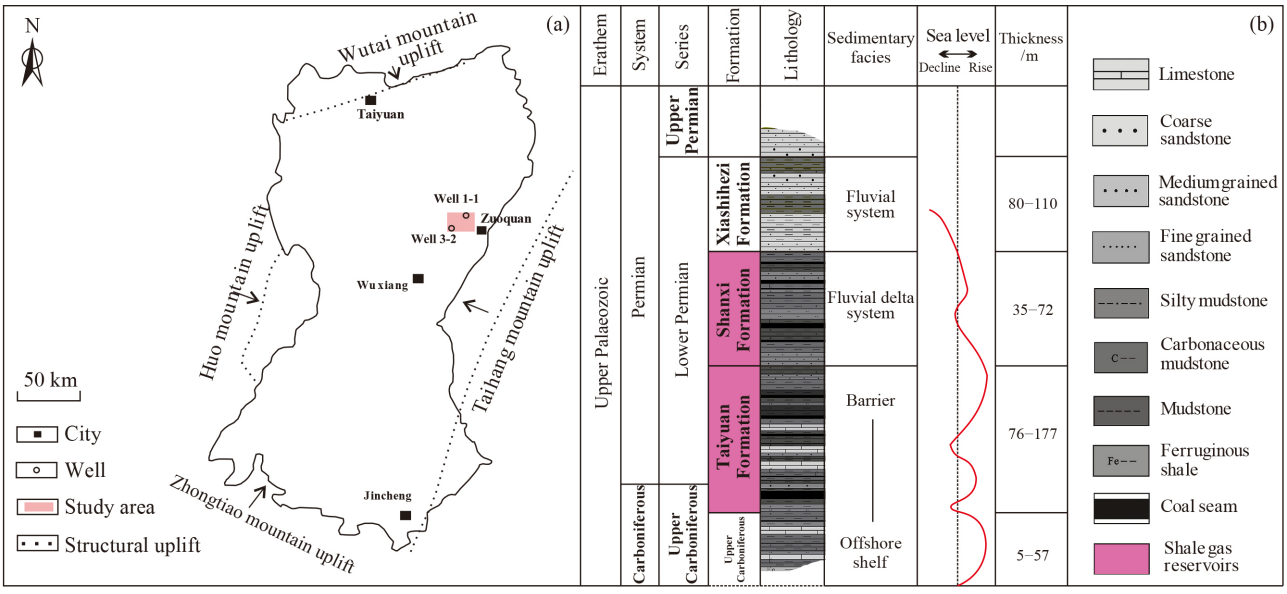

Fig. 1 (a) Locations of studied wells in the Qinshui Basin, and (b) stratigraphic column for the upper Carboniferous-upper Permian strata of the Zuoquan area (modified after Li et al. (2018a) and Xi et al. (2018)). The coal-bearing shales are mainly developed in the Taiyuan and Shanxi formations.

Table 1 Basic information, TOC contents, R_o values, and mineralogical compositions of the studied shale samples

Well	Sample	Formation	TOC/%	R_o[a)]/%	Mineral composition/%								
					Quartz	Feldspar	Siderite	Pyrite	Anatase	Others[b)]	I/S	Kaolinite	Chlorite
Well 1-1	1	Shanxi Fm.	1.96	–	47.94	1.08	0	0	2.35	0	36.87	6.07	3.73
	2	Shanxi Fm.	8.54	2.59	47.74	0	1.28	0	0	1.37	33.26	6.16	1.64
	3	Taiyuan Fm.	2.09	–	48.96	0	0	0	1.27	9.20	28.47	8.47	1.54
	4	Taiyuan Fm.	3.84	–	38.85	0.67	0	0	1.44	0	48.66	5.53	1.11
	5	Taiyuan Fm.	16.1	2.55	33.06	1.76	2.52	0	1.51	0	40.47	2.70	1.80
Well 3-2	6	Shanxi Fm.	5.24	–	29.85	8.05	0	0	0	15.45	40.58	0	0.83
	7	Shanxi Fm.	0.92	–	69.16	0	0	4.46	0	0	9.80	11.87	3.79
	8	Shanxi Fm.	12.4	2.70	34.16	0	7.45	0	0	0	30.63	15.36	0
	9	Shanxi Fm.	0.96	–	58.43	0	17.33	0	0	0	10.85	12.43	0
	10	Shanxi Fm.	1.01	–	45.14	0	0	1.39	0	0	15.74	36.73	0
	11	Taiyuan Fm.	1.93	–	49.04	0	0	23.54	0	0	8.06	17.44	0
	12	Taiyuan Fm.	11.2	3.16	32.16	0	3.20	0	0	0	25.36	28.48	0
	13	Taiyuan Fm.	2.3	–	48.65	0	0	0	0	0	21.19	23.44	4.41
	14	Taiyuan Fm.	2.4	–	22.84	0	10.25	1.37	1.76	0	28.28	27.67	5.53
	15	Taiyuan Fm.	3.21	–	42.00	0	0	0	0	0	15.60	39.19	0

Notes: a) –: not measured; b) Others include calcite, anhydrite, and hematite.

et al., 2008). Natural desorption was conducted at the temperature of the reservoir, and the obtained gas was categorized as the desorbed gas. After natural desorption, samples were crushed for 2−4 h at the reservoir temperature and residual gas was obtained. Typically, the lost gas content is calculated using the USBM (US Bureau of Mines) linear regression method (Zhou, 2002; Deng et al., 2008; Sun et al., 2018). Due to the greater burial depth, a higher proportion of free gas may be lost during the uplifting of core samples, and the lost gas contents calculated by the USBM method may be lower than actual values (Wang et al., 2020b). Previous authors have suggested the polynomial regression method to calculate the lost gas contents of deeply-buried gas shale reservoirs (Sun et al., 2018), and this method was also used in our study. The lost gas contents were calculated by the polynomial regression fitting method of the first 2 h of data from natural desorption (Fig. 2). The GIP content is the sum of the desorbed gas, residual gas and lost gas.

2.2.2 SEM observation

The shale samples were first mechanically polished and then further polished by an argon ion milling system IM4000 to obtain highly smooth surfaces. Scanning electron microscope (SEM) observation of the polished samples were conducted on a high-resolution cold field emission scanning electron microscopy (Hitachi S-8000). Imaging was performed at 1−10 kV and a working distance of 1.5−15 mm under a vacuum.

2.2.3 Total organic carbon and R_o measurements

After the removal of carbonate minerals with 5% HCl, the total organic carbon (TOC) content of the powdered samples were measured with the total carbon and sulfur Leco CS-200 analyzer. The TOC contents were calculated by the peak area of CO_2 generated from the combustion of OM and calibrated by carbon in steel (TOC = 0.812 ± 0.006%) (Wang et al., 2013).

The vitrinite reflectance (R_o) was determined on polished shale samples using a 3Y-Leica DMR XP microphotometer. The microscope was calibrated with a cubic zirconia reference (R_o = 3.11%) and an optical black (zero), and the measurements were conducted in oil immersion under incident light using a 50 × /0.85 oil lens. In each sample, 50 different vitrinite particles were randomly selected for measurements, and the data were averaged.

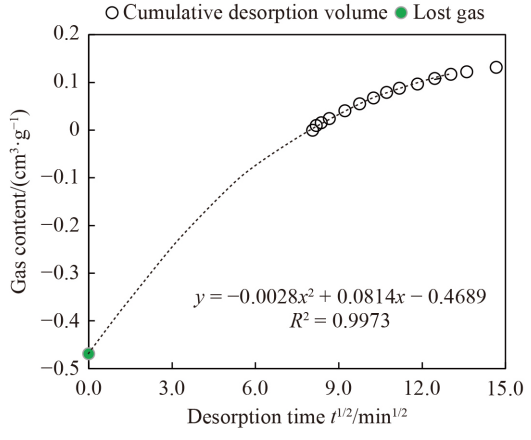

Fig. 2 Plot showing the desorption curve and the fitting calculation of the lost gas content of sample 13. The results show that the lost gas content is 0.47 m^3/t, which is calculated by the polynomial regression method based on the first 2 h of data from the natural desorption process.

2.2.4 X-ray diffraction

X-ray diffraction (XRD) measurements of powdered whole-rock samples were conducted on a Bruker D8 Advance X-ray diffractometer equipped with a Cu-target tube and a curved graphite monochromator, operating at 40 kV and 30 mA. Samples were step-scanned from 3° to 85° with a step size of 0.04° (2θ), and the mineral composition was semiquantitatively determined using peak area integration approach with correction for Lorentz polarization (Pecharsky and Zavalij, 2008).

2.2.5 Porosity

Small cylindrical cores with a diameter of 25 mm and a length of 20 mm were drilled from the selected shale core samples. The cores were first dried at a temperature of 110°C to remove any moisture and weighed, and then porosity was determined using skeletal density and apparent density differences. Skeletal density was measured with a helium pycnometer from Quantachrome, the Ultrapyc 1200e, and apparent density was measured on a hydrometer (DAHO-120M) by the sealing paraffin method. The analytical procedures used in the present study were detailed by previous authors (Tian et al., 2013).

2.2.6 Low-pressure N_2 adsorption experiments

Approximately 2 g of crushed sample (60−80 mesh) was dried at 110°C in an oven for 24 h to remove moisture and volatile materials. Each sample was then analyzed for pore volume using low-pressure N_2 adsorption on a Micromeritics ASAP 2020 analyzer. The measured relative pressures were 0.005−0.995 and the tested temperature was 77.35 K (liquid nitrogen temperature). Pore volume (PV) and specific surface area (SSA) were calculated from the adsorption isotherm using the Barrett-Joyner-Halenda (BJH) model (Barrett et al., 1951) and the modified Brunauer–Emmett–Teller (BET) equation (Romero-Sarmiento et al., 2014; Tian et al., 2015). In

general, N_2 adsorption permits the identification of pores ranging from 1.7 to 100 nm.

3 Results

3.1 Bulk organic geochemistry

The TOC content of the studied shale samples vary from 0.92% to 16.1%, averaging 4.94% (Table 1). The R_o value of the studied shale samples ranges from 2.55% to 3.16% (Table 1), suggesting that the shale is currently in the thermally high- and overmature stage.

3.2 Mineralogical compositions

The studied shale is dominated by quartz and clay (Table 1). The quartz content ranges from 22.84% to 69.16%, with an average of 43.20%; the total clay content varies from 23.27% to 61.49%, with an average of 43.98%. Some shale samples contain small amounts of feldspar, pyrite, siderite, and anatase, and their contents are generally less than 10%. Few shale samples also contain a small quantity of calcite, anhydrite, and hematite. The species of clay minerals are dominated by I/S, followed by kaolinite and chlorite. The I/S contents range from 8.06% to 48.66% (average 26.25%), and the kaolinite content varies from 0 to 36.37% (average 16.10%). The chlorite content is usually less than 5.53%. Overall, the studied coal-bearing shales are characterized by lower quartz contents and higher clay contents relative to typical marine shales (Fig. 3).

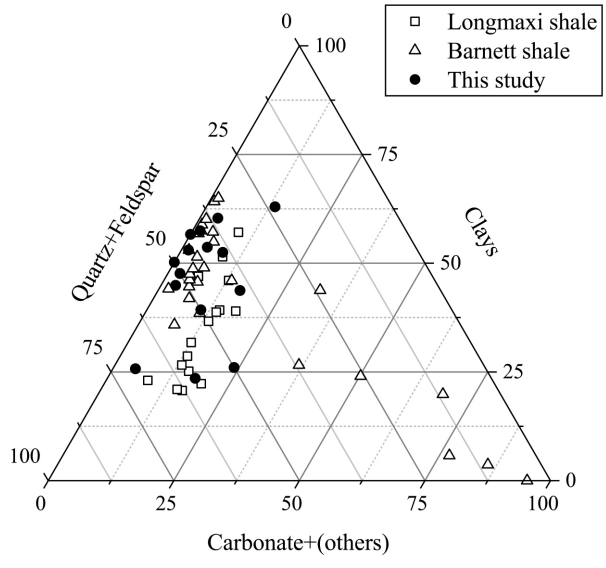

Fig. 3 Ternary plot of quartz + feldspar, carbonate, and clays for the studied shale samples. The data of the Barnett shale and the Longmaxi shale are from Jarvie et al. (2007) and Sun et al. (2020a), respectively. Carbonate = dolomite + calcite + siderite.

3.3 Porosity, pore types and pore structure characteristics

The measured porosity values of the studied shale samples range from 2.00% to 9.47%, averaging 5.12% (Table 2). SEM observations reveal that the pores in the studied shale samples mainly included OM-hosted pores, clay-hosted pores, mineral interparticle pores, and microcracks (Fig. 4). In some OM fragments, original structures can be clearly observed, but rare organic pores are visible at this scale (Fig. 4(a)). Few isolated organic pores can also be observed, and these pores display round shapes (Figs. 4(b)−4(e)). Some organic pores are connected (Fig. 4(d)). Clay-hosted pores are widely developed in the studied shale samples, and can be observed in the clay-OM associations, clay aggregates, and clay platelets (Figs. 4(f)−4(j)). Abundant elongated and irregular clay-hosted pores occurr within the I/S (Figs. 4(g) and 4(j)). Slit-shaped intergranular pores widely occur between kaolinite aggregates (Fig. 4(i)). Mineral interparticle pores are mainly developed between quartz grains (Fig. 4(k)), which are also usually observed in the siderite and pyrite aggregates (Figs. 4(k) and 4(l)). Microcracks were usually visible along the margins of quartz grains in quartz-rich shale samples (Fig. 4(k)).

The SSA values of the studied shale samples range from 2.05 to 17.88 m^2/g, with an average of 11.29 m^2/g. The PV values vary from 0.60×10^{-2} to 3.37×10^{-2} cm^3/g, with an average of 2.16×10^{-2} cm^3/g. The average pore size (APS) values range from 5.38 to 13.55 nm, averaging 8.57 nm (Table 2).

3.4 GIP content

The contents of lost gas, residual gas, desorbed gas and GIP of the studied shale samples are presented in Table 3.

Table 2 Porosity and pore structure parameters of the studied shale samples

Sample	Porosity/%	SSA/($m^2 \cdot g^{-1}$)	PV/($\times 10^{-2}$ $cm^3 \cdot g^{-1}$)	Average pore size/nm
1	2.13	10.80	2.54	9.56
2	4.62	6.76	1.81	10.68
3	6.03	8.41	1.76	8.36
4	6.81	17.88	3.37	7.55
5	3.93	13.77	2.91	8.45
6	4.74	12.55	2.71	6.29
7	3.18	9.46	2.63	11.13
8	2.66	9.13	0.70	13.14
9	2.00	2.05	0.60	13.55
10	5.04	13.24	2.26	6.84
11	9.74	10.25	1.99	7.85
12	6.50	10.35	1.71	6.60
13	6.16	13.90	2.61	7.51
14	4.90	13.60	1.83	5.38
15	6.42	17.17	2.94	5.68

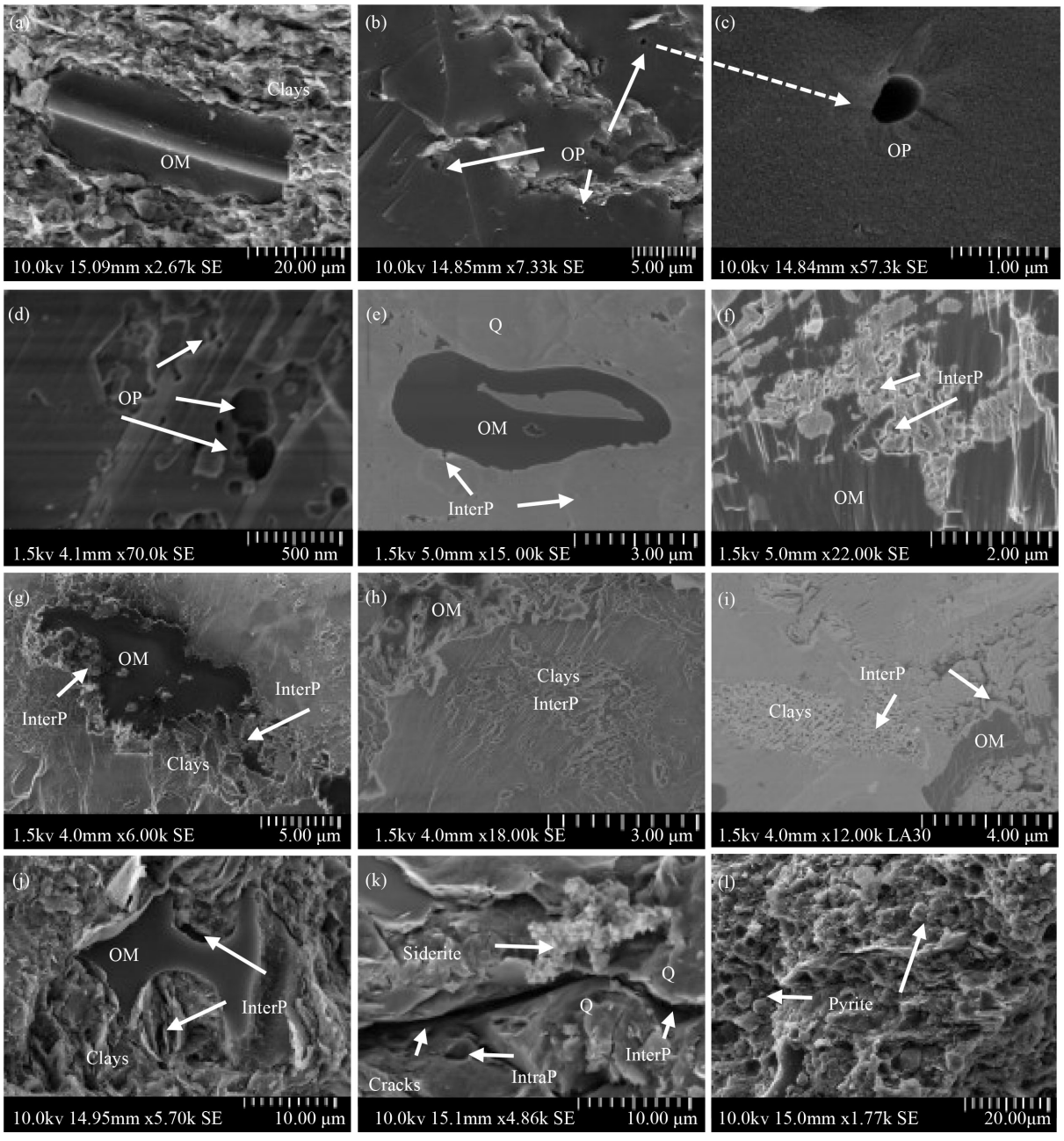

Fig. 4 SEM photographs illustrating various minerals and pore types in the studied shales. (InterP = interparticle pore; IntraP = intraparticle pore; OP = organic pore; Q = quartz). (a) Terrigenous OM fragments are surrounded by clay minerals and retain original plant structures, but organic pores are lacking; (b) and (c) isolated organic pores within the OM, a close-up of a rounded organic pore is presented in panel (c); (d) organic pores with rounded shapes occur within the OM, and some of them are partially connected; (e) pores are developed between the OM and clay minerals; (f) interparticle pores of clay minerals and interparticle pores between clays and organic matter; (g) organic matter surrounded by clay minerals and intergranular pores are developed between them; (h) slit interparticle pores between clay minerals; (i) slit pores between kaolinites; (j) terrigenous OM fragments retains original plant structures without pores, but interparticle pores are developed between the OM and clays, as well as clay platelets; (k) inter-particle pores are developed between quartz grains, and a microcrack can be observed along the margin of quartz grains. Isolated intraparticle pores are also developed within quartz grains; (l) pyrite aggregates surrounded by clay minerals.

The GIP content ranges from 0.30 to 2.28 m^3/t, with an average of 1.32 m^3/t. The desorbed gas contents vary from 0.19 to 1.98 m^3/t, with an average of 0.94 m^3/t. The residual gas contents are in the range of 0.01−0.56 m^3/t (average = 0.21 m^3/t). The lost gas content ranges from 0.01 to 0.66 m^3/t, with an average of 0.17 m^3/t. The desorbed gas, lost gas, and residual gas account for 44.32%−94.13%, 1.07%−33.65%, and 1.13%−32.49% of the GIP, respectively (Fig. 5). Thus, the desorbed gas dominates the GIP content.

Table 3 Gas contents of the studied shale samples

Sample	Desorbed gas/ ($m^3 \cdot t^{-1}$)	Residual gas/ ($m^3 \cdot t^{-1}$)	Lost gas/ ($m^3 \cdot t^{-1}$)	GIP/ ($m^3 \cdot t^{-1}$)
1	1.16	0.03	0.08	1.27
2	1.98	0.04	0.26	2.28
3	0.35	0.01	0.01	0.38
4	1.49	0.02	0.66	2.17
5	1.45	0.03	0.07	1.55
6	1.11	0.02	0.05	1.18
7	0.19	0.10	0.01	0.30
8	1.12	0.56	0.05	1.74
9	0.34	0.17	0.03	0.53
10	0.57	0.29	0.44	1.30
11	0.78	0.39	0.10	1.28
12	1.71	0.46	0.02	2.19
13	0.77	0.39	0.47	1.63
14	0.66	0.33	0.15	1.14
15	0.48	0.24	0.20	0.92

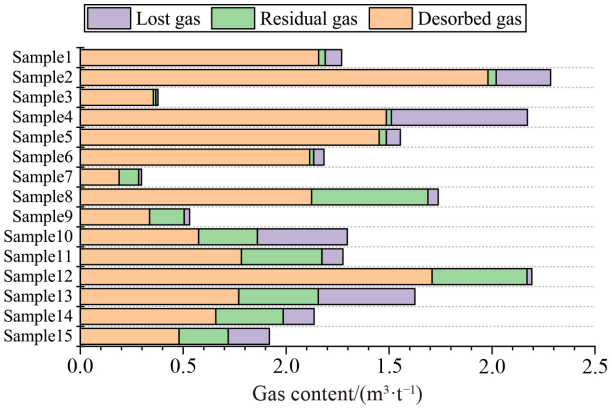

Fig. 5 GIP compositions of the studied shale samples.

4 Discussion

4.1 Influence of OM and mineral compositions on porosity

Numerous studies have suggested that the pore evolution of shales is controlled by both primary sedimentary compositions, including the OM and inorganic mineralogical composition, and subsequent diagenetic processes (Loucks et al., 2009; Mastalerz et al., 2013). For overmatured marine shales, the TOC content has always positively correlated with the porosity within a certain TOC range, indicating that organic pores are the predominant pore type and the porosity is directly controlled by the TOC content (Tian et al., 2013; Sun et al., 2020a). Such a significant correlation between the TOC content and porosity cannot be observed in this study (Fig. 6(a)). Within the TOC range of 0.92%–5.24%, the TOC content displays a weak positive correlation with porosity values. The porosity began to diminish for TOC values in excess of 8.54% (Fig. 6(a)). A similar trend also occurs in marine shales and coal-bearing shales in the Yangtze Block, South China (Milliken et al., 2013; Pan et al., 2015; Teng et al., 2021). Such a reduction in porosity values has usually been attributed to pore collapse due to mechanical compaction (Milliken et al., 2013; Furmann et al., 2016). Therefore, TOC contents $\leqslant$ 5.24% can be defined as the uncompacted stage of OM in this study. Since the data sets of TOC values ranging from 5.24% to 8.54% are lacking in our study, the accurate turning point of porosity is very hard to predict.

It should be noted that the correlation coefficient between the TOC content and porosity in the coal-bearing shales is significantly lower than that in the lower Paleozoic marine shales from south China (Tian et al., 2013; Sun et al., 2020a; Xi et al., 2021). Such a weak correlation can also be found in the coal-bearing shales from the Qinshui Basin (Zhang and Fu, 2018) and other basins, e.g., the Ordos Basin (Tang et al., 2016) and the

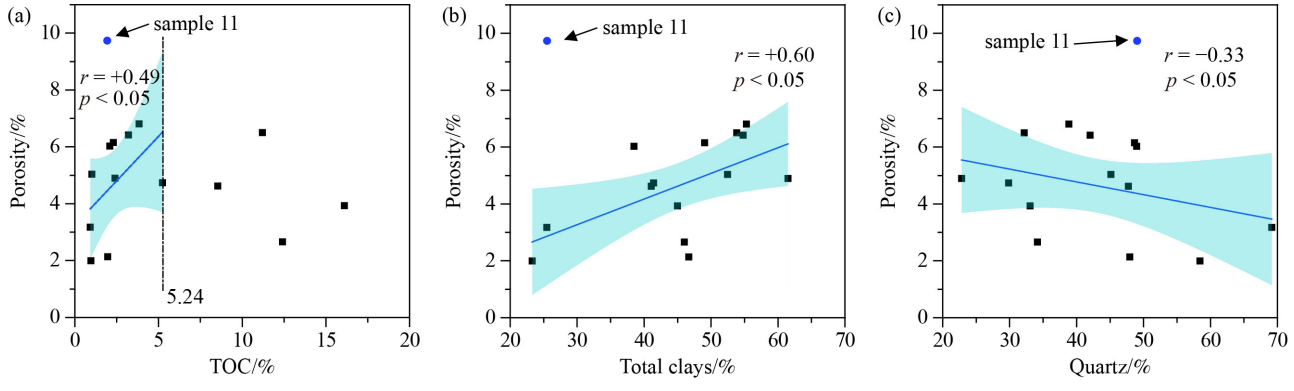

Fig. 6 Cross-plots of (a) porosity versus TOC values, (b) porosity versus total clay contents, and (c) porosity versus quartz contents. Regression lines (solid) with 95% confidence intervals ($p < 0.05$) (cyan zones) and Pearson correlation coefficient (r) are shown.

Sichuan Basin (Luo et al., 2019), which may be mainly attributed to the poor development of organic pores in gas-prone kerogen (i.e., type III). In contrast, organic pores have been suggested to be widely developed in marine shales with oil-prone kerogen (type I-II) (Bowker, 2007; Chalmers et al., 2012). In our study, SEM-visible organic pores seem to be not well developed (Figs. 4(a)−4(f)). Due to the limitations of SEM observation in nanopores (generally > 5−10 nm), micropores and small mesopores in OM are very hard to be observe (İnan et al., 2018). However, micropores and small mesopores might be mainly developed in the OM of coal-bearing shales, which have been widely reported in many sedimentary basins (e.g., the Ordos Basin (Qiu et al., 2021), Sichuan Basin (Yang et al., 2019), and Qinshui Basin (Xi et al., 2017a)) in China.

An outlier shale sample (i.e., Sample 11) displays a low TOC content (1.93%) but high porosity (9.74%) (Fig. 6(a)), which may result from a higher content of pyrite (as high as 23.54%). As mentioned above, a large volume of interparticle pores is developed between pyrites (Fig. 4(l)). The porosity values show a moderate positive correlation with total clay contents (r = + 0.60, n = 14; excluding an outlier sample) (Fig. 6(b)), which can also be observed in coal-bearing shales from the Ordos Basin (Qiao et al., 2020) and Sichuan Basin (Yang et al., 2017; Chen et al., 2021). The species of clay minerals in the studied shales mainly include kaolinite and I/S (Table 1). Previous authors have found that the pore diameters of kaolinite and I/S are dominantly 10−70 nm, < 6 nm and 20−70 nm (Ji et al., 2014). Thus, clay-hosted pores greatly contribute to shale porosity. Yang et al. (2017) also believed that the porosity of coal-bearing shales in the Sichuan Basin is mainly contributed by clays rather than the OM.

As one of the major brittle minerals in shales, quartz can esist to burial compaction. A high proportion of brittle minerals can form a rigid framework that can be favorable for the protection of organic pores, which has been widely reported in marine shales (Milliken et al., 2013; Zhang et al., 2013; Furmann et al., 2016).

In our study, the quartz contents of the studied shales display no correlation with the porosity values (Fig. 6(c)), which can be attributed to the following reasons. The quartz may be of terrigenous origin rather than biological origin, with relatively low contents in the studied shales, which plays a dilution role in the TOC and clay mineral contents, as suggested by the moderate negative correlation between the quartz and TOC or clay contents (Figs. 7(a) and 7(b)). To explore the effect of quartz on the porosity, TOC-normalized and clay-normalized parameters (i.e., porosity/TOC ratio and porosity/clay ratio) are introduced in our study; these parameters refer to the relative contribution of inorganic porosity and organic porosity to total porosity, respectively. A moderate positive correlation between the quartz content and the porosity/TOC ratio can be observed in our studied shales (r = + 0.61; n = 13; excluding outliers) (Fig. 7(c)), indicating that inorganic porosity may be protected by rigid frameworks formed by quartz grains from compaction. The lack of a relationship between the quartz content and the porosity/clay ratio probably suggests that the development of organic pores is not associated with quartz (Fig. 7(d)), which also supports a terrigenous origin of quartz.

4.2 Influence of OM and mineral compositions on pore structures

In general, the TOC contents display a good positive relationship with the pore structure parameters (e.g., SSA and PV) of marine shales (Milliken and Olson, 2017; Tang et al., 2020). In our study, the TOC contents have moderately correlated with the SSA and PV with TOC contents less than 5.24% (Figs. 8(a) and 8(b)), suggesting that the OM during the uncompacted stage of shales has a certain contribution to total SSA and PV. Such an increasing trend disappears with increasing TOC contents (Figs. 8(a) and 8(b)).

A moderate positive correlation between clay contents and SSA values (r = + 0.71) indicates that clay minerals have complex surface areas and are a major contributor to the SSA of total pores (Fig. 8(c)). Although the quartz contents are not correlated with the SSA and PV values (not shown in this study), they display weak-moderate positive relationships with the TOC-normalized pore structure parameters (Fig. 8(d)), indicating that quartz may play a positive role in the protection of nanopores in the studied shales to some extent. Moreover, only a part of the pore volume is measured by N_2 adsorption, which cannot fully represent the total pore volume of the studied shale samples.

In the uncompacted stage of organic matter (TOC ⩽ 5.24%), there is a moderate negative correlation (r = −0.59) (Fig. 9(a)) between the TOC content and APS, probably implying that OM is mainly composed of micropores. A moderate negative correlation between clay contents and APS values can be observed in our study (r = −0.63) (Fig. 9(b)). Previous authors have found that pores with diameters < 20 nm in shales would significantly increase with the increasing clay contents, while larger pores (> 20 nm) would not significantly increase (Yuan et al., 2021). Thus, the increase of clay contents gradually decreases the APS values of studied shales. A moderate positive correlation (r = + 0.54) between quartz contents and APS values is also observed (Fig. 9(c)), further indicating the role of quartz grains in the preservation of larger nanopores.

4.3 Factors that influence the GIP contents

As mentioned above, the porosity and pore structures of coal-bearing shales in this study are mainly controlled by

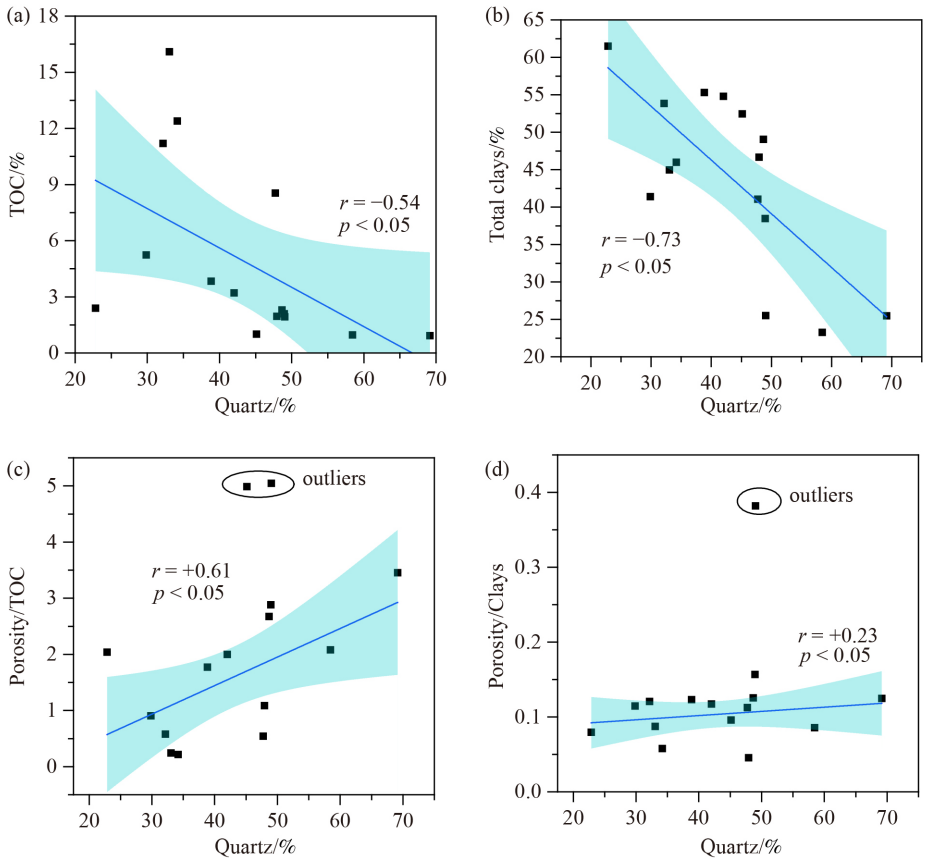

Fig. 7 Cross-plots of the quartz contents versus (a) TOC values, (b) clay contents, (c) porosity/TOC ratios, and (d) porosity/clays ratios of the studied shale samples.

clay contents, followed by TOC contents. The porosity and pore structure are directly related to shale GIP contents; therefore, the influences of shale compositions and pore characteristics on the GIP contents should be explored.

4.3.1 OM and mineral compositions

In this study, the GIP contents show a moderate positive correlation with TOC contents (Fig. 10(a)). Such a positive relationship has also been reported in coal-bearing shales from the south–north China Basins (Li et al., 2020a). The GIP contents appear to be lower in the high-TOC shale samples (TOC > 8.5%) (Fig. 10(a)), which may have resulted from the collapse of pores during burial compaction. The GIP contents have a weak positive correlation with total clay contents (Fig. 10(b)), implying that clay minerals have a certain contribution to gas contents. However, a weak negative correlation between the GIP and quartz contents is observed (Fig. 10(c)), which may be attributed to two potential factors. First, quartz contents display negative correlations with TOC and clay contents (Figs. 7(a) and 7(b)), suggesting that terrigenous quartz grains play a dilution role in the OM and clay accumulations. Second, interparticle pores between quartz grains mainly consist of large pores (Ge et al., 2020), which have weak adsorption capacities for methane (Wang et al., 2020c; Shi et al., 2021) but could provide a certain volume of storage space for free gas. However, the gas composition of the studied shales is mainly adsorbed gas, so the control of quartz contents on the GIP contents is relatively weak.

These results show that the GIP contents of the studied shales are mainly controlled by the TOC and total clay contents, which is different from marine gas-bearing shales (Strąpoć et al., 2010; Milliken et al., 2013; Sun et al., 2020a). For marine shales, the GIP contents are always positively correlated with TOC contents (Strąpoć et al., 2010; Zheng et al., 2019), while they generally display no positive relationships with total clay contents (Li et al., 2022).

It is widely accepted that the total gas of shales consists of lost gas, desorbed gas, and residual gas (Liang et al., 2020b; Xu et al., 2020a). Lost gas can be considered free gas in shale; residual gas is mostly occur in the form of adsorbed gas; and desorbed gas consists of both free gas and adsorbed gas (Li et al., 2020b). The adsorbed + residual gas contents of the studied shales have a moderate positive correlation with the TOC contents but display no correlation with the lost gas contents (Fig. 11(a)),

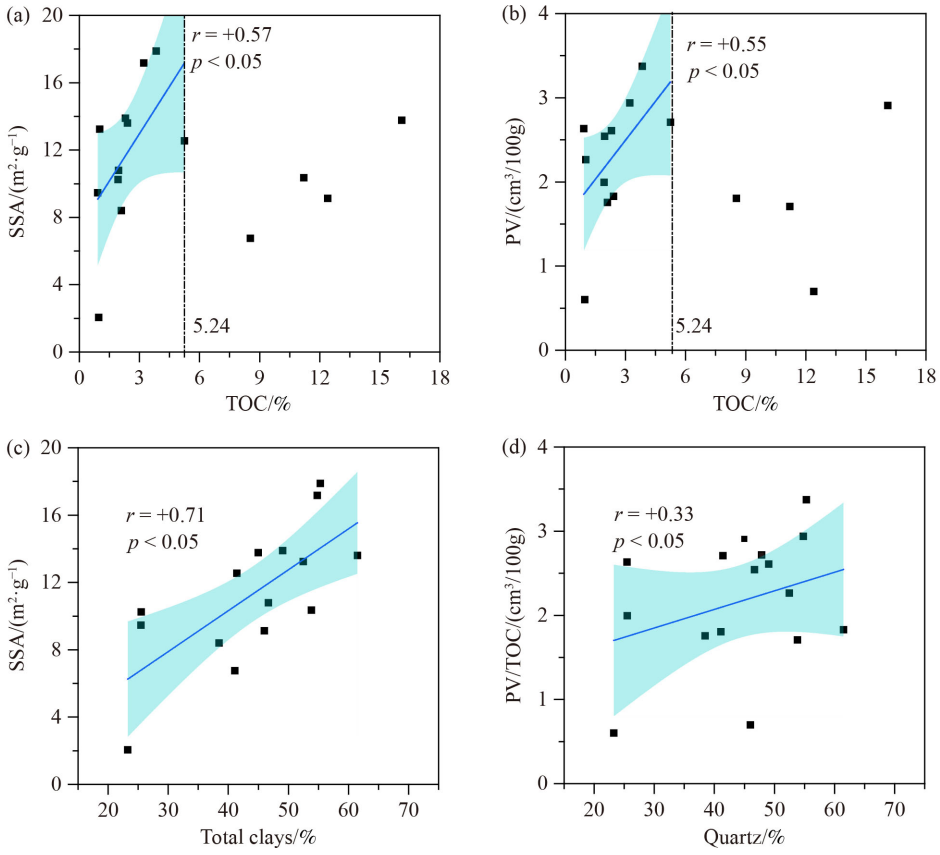

Fig. 8 Cross-plots of (a) TOC versus SSA, (b) TOC versus PV, (c) total clay contents versus SSA, and (d) quartz contents versus the PV/TOC ratios of the studied shale samples.

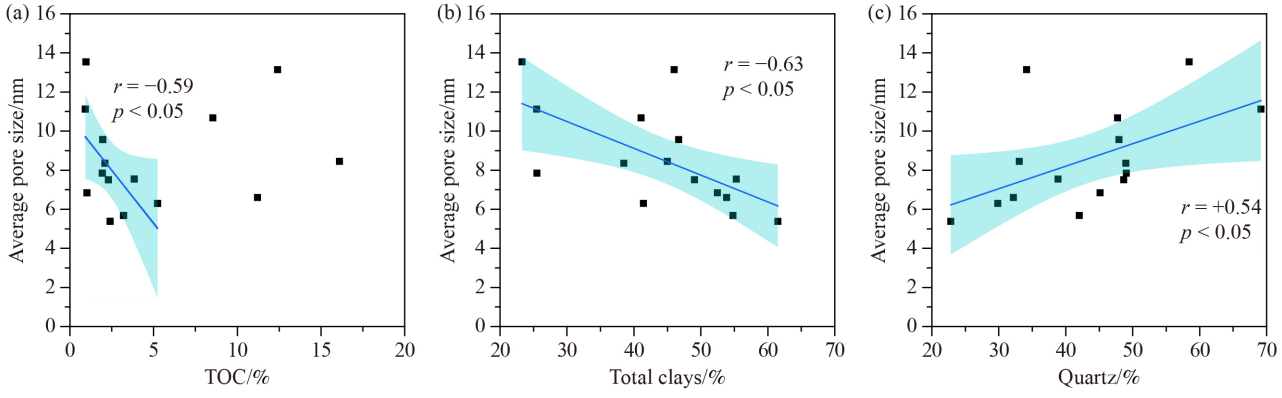

Fig. 9 Cross-plots of the APS values versus (a) TOC contents, (b) total clay contents, and (c) quartz contents of the studied shale samples.

suggesting greater controls of the OM on the adsorbed gas. Lost gas and adsorbed + residual gas contents display weak positive correlations with total clay contents (Fig. 11(b)), but the clays have greater controls on lost gas, implying that the methane occurs in clays mainly as free gas. The adsorbed + residual gas contents of the studied shales show a moderate positive correlation with the I/S contents (Fig. 11(c)), while it does not correlate with the kaolinite + chlorite contents (Fig. 11(d)), indicating that the I/S is the major type of clay minerals of the studied shales and plays a leading role in methane adsorption relative to other clay species. Previous studies have also shown that the methane adsorption capacity of I/S is significantly stronger than that of kaolinite and chlorite (Ji et al., 2014). In general, illite, smectite, and I/S could provide greater SSA values than kaolinite, thus affecting adsorption capacity.

4.3.2 Porosity and pore structures

Numerous studies have showed that porosity and pore structures provide storage spaces for methane and

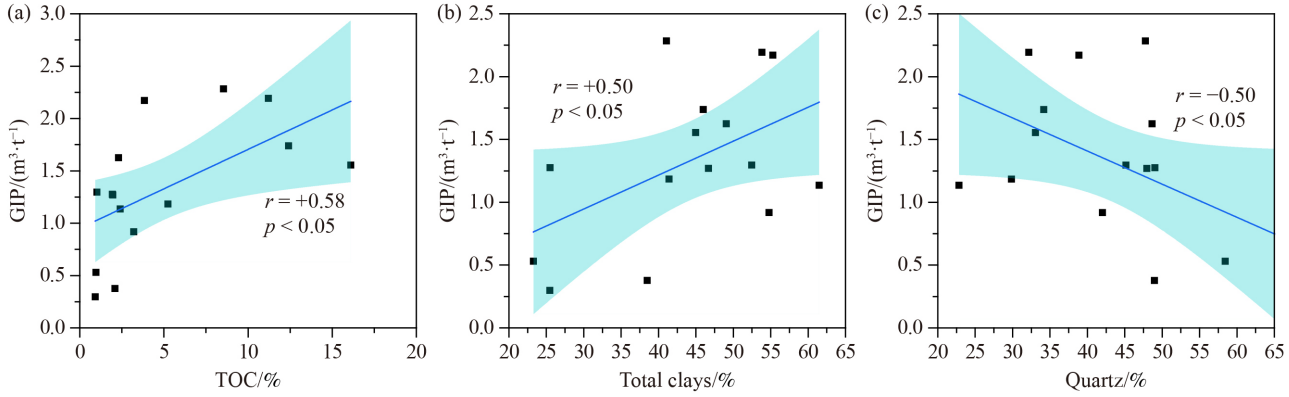

Fig. 10 Cross-plots of (a) GIP versus TOC contents, (b) GIP versus total clay contents, and (c) GIP versus quartz contents.

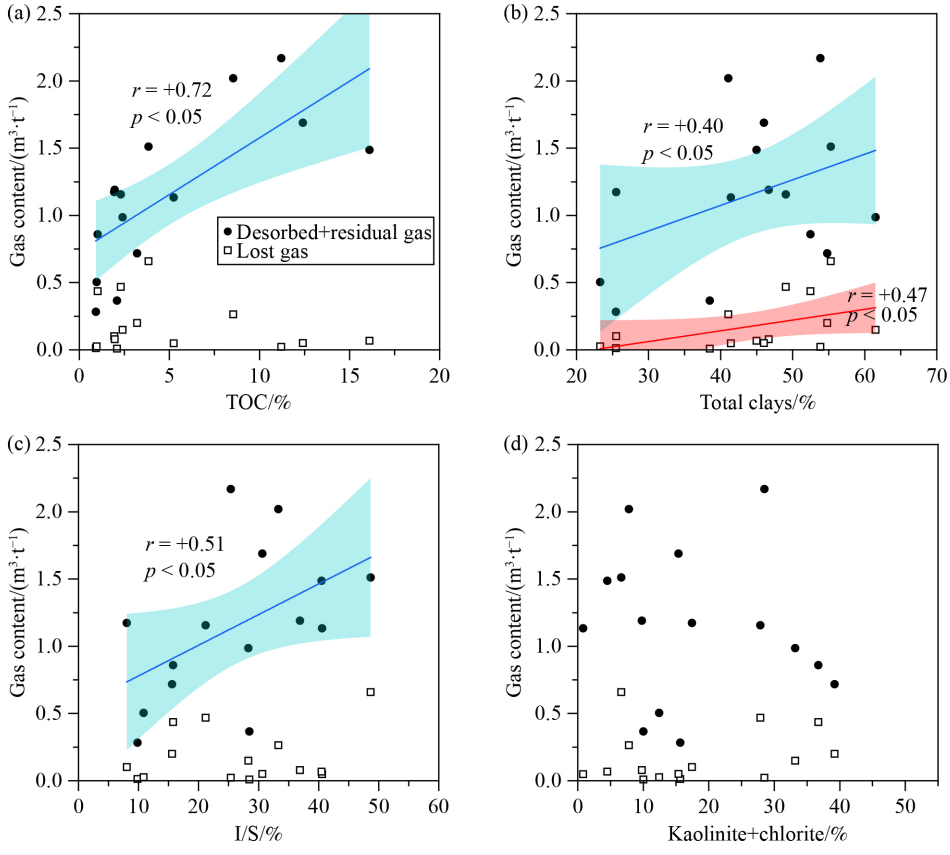

Fig. 11 Cross-plots of gas contents versus (a) TOC contents, (b) total clay contents, (c) I/S contents, and (d) the kaolinite + chlorite contents of the studied shale samples.

influence the adsorption capacity of methane, thus directly controlling the GIP contents of shales (Curtis, 2002; Jarvie et al., 2007; Ross and Bustin, 2008). However, no positive correlations between GIP contents and the porosity or pore structure parameters (PV, SSA, and APS) are shown in all studied shale samples (Fig. 12).

Zhong et al. (2020) collected data from 695 coal-bearing shale samples from the Qinshui Basin and found that 84.97% of shale samples displayed TOC values less than 4%. Thus, the coal-bearing shales in the Qinshui Basin are characterized by lower TOC contents. As mentioned above, the larger organic pores in the high-TOC shale samples would be strongly affected by burial compaction, thus resulting in the alteration of pore structures. Thus, it is necessary to explore the relationship between the GIP contents and the porosity or pore structure parameters (PV, SSA, and APS) in the low-TOC shale samples (TOC $\leqslant$ 5.24%) (Fig. 13). The GIP contents display a weak positive relationship with the porosity and have a moderate correlation with the SSA values and PV values, respectively (Fig. 13), suggesting that total gas is dominated by adsorbed gas, which is

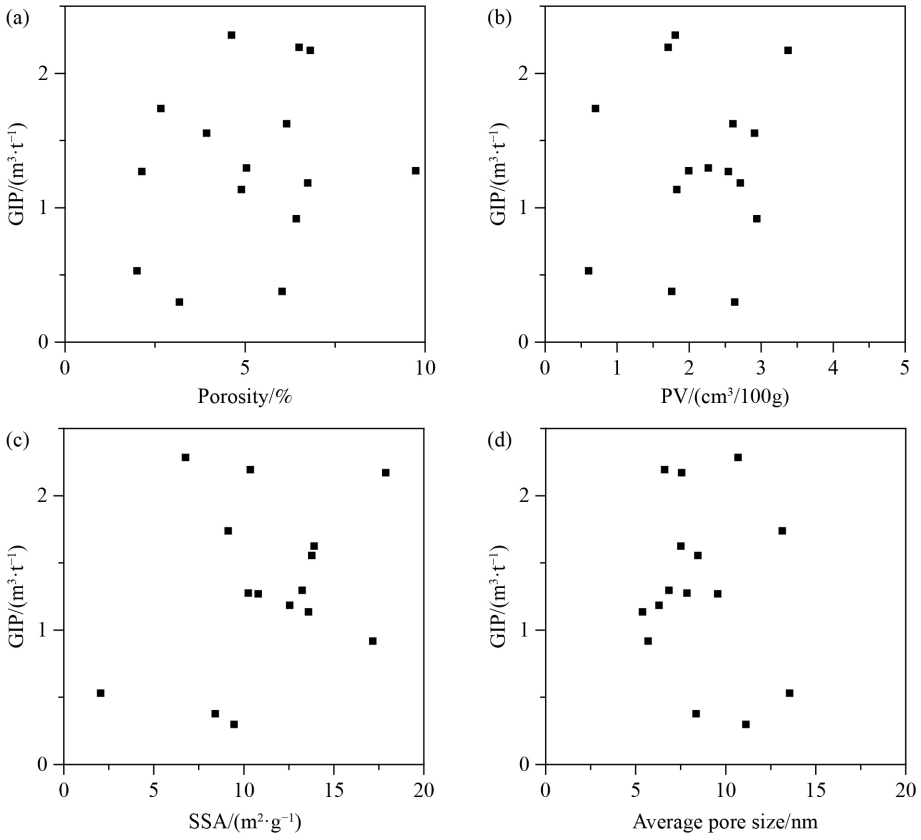

Fig. 12 Cross-plots of GIP contents versus (a) porosity values, (b) PV values, (c) SSA values, and (d) APS values of the studied shale samples.

consistent with previous studies (Ma et al., 2021).

In marine shales, the porosity and pore structure parameters are mainly controlled by the TOC contents, which have been revealed by numerous studies (Milliken et al., 2013; Zhao et al., 2018; Sun et al., 2020a; Xu et al., 2020b). Compared with marine shales, the GIP contents of the studied coal-bearing shales are relatively low, and the relationships between the GIP contents and the porosity or several pore structure parameters are weak, implying that the major factors controlling the GIP contents of coal-bearing shale are more complex than those of marine shale. The pore spaces of coal-bearing shales are primarily provided by clay minerals, followed by OM. In general, the clay-hosted pores are strongly hydrophilic and easily occupied by water molecules (Borysenko et al., 2009; Cheng et al., 2017; Guo et al., 2021; Sun et al., 2021). The clay surfaces may be partly or fully adsorbed by water molecules, so the adsorbed gas contents should be reduced due to the decrease of methane adsorption sites (Cheng and Huang, 2004; Merkel et al., 2015; Tang et al., 2020). Although the water contents of shale samples are not measured in this study, we believe that the pores of coal-bearing shales are influenced by water contents to some extents, thus resulting in lower GIP contents and poor correlations between the GIP contents and porosity or pore structure parameters.

In addition, a weak negative correlation between the GIP contents and APS values was observed in this study (Fig. 13(d)). With the increase of clay contents, the slit-shaped clay-hosted pores are increased in the studied shales, thus leading to the increase of porosity, PV, and ASS values (e.g., Fig. 6(b)). However, the increasing proportions of slit-shaped pores would lead to a decrease in the APS values and an increase in GIP contents.

5 Conclusions

Major factors influencing the GIP contents in organic-rich coal-bearing shales from the Qinshui Basin have been studied, and the following conclusions can be drawn.

1) The coal-bearing shales are enriched in clay minerals, which are mainly composed of I/S, followed by kaolinite. Interparticle pores hosted in clay minerals are commonly developed in shales, while SEM-visible OM-hosted pores are not well developed.

2) The porosity, PV and SSA of coal-bearing shales were mainly contributed by clay minerals, followed by OM, which can provide storage spaces and adsorption sites for methane, thus influencing the gas contents.

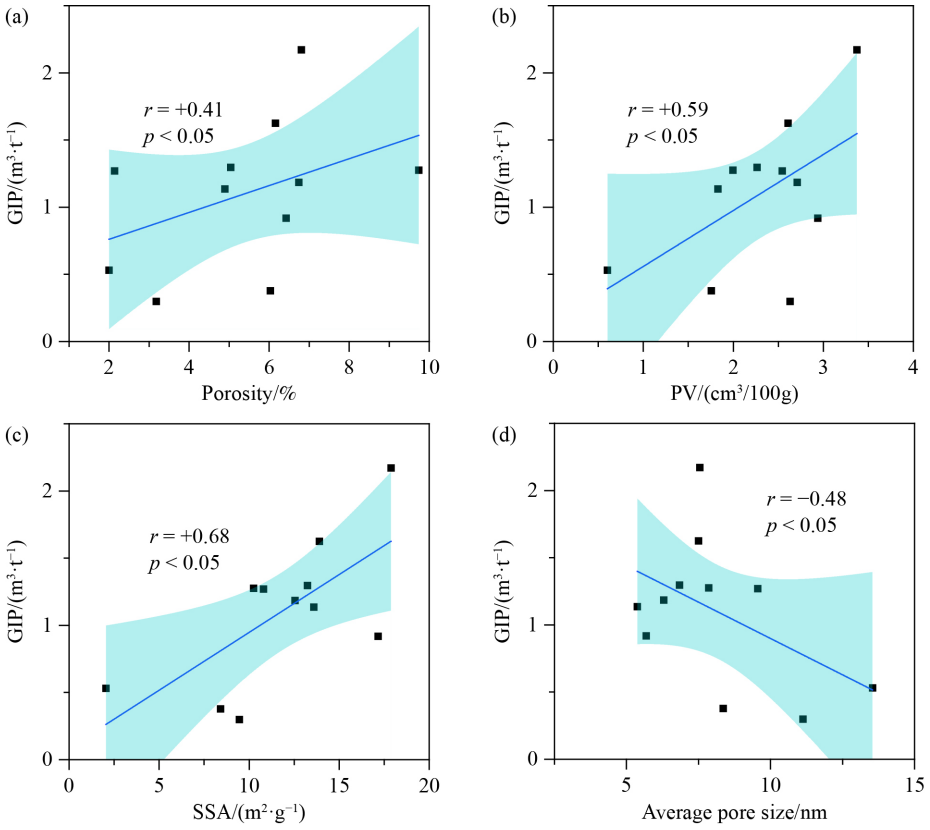

Fig. 13 Cross-plots of GIP contents versus (a) porosity values, (b) PV values, (c) SSA values, and (d) APS values of the studied shale samples during the uncompacted stage (TOC ⩽ 5.24%).

3) The GIP contents of coal-bearing shales range from 0.30 to 2.28 m^3/t, with an average of 1.32 m^3/t, which are dominated by the desorbed gas contents. The major factors influencing the GIP contents of coal-bearing shales include both TOC and clay contents. Among all clay species, I/S plays a leading role in methane adsorption, which is favorable for methane enrichment in shales.

Acknowledgments This study was jointly supported by the National Natural Science Foundation of China (Grant No. U1810201) and the Science and Technology Department of Shanxi Province, China (No. 20201101003).

References

Barrett E P, Joyner L G, Halenda P P (1951). The determination of pore volume and area distributions in porous substances. I. Computations from nitrogen isotherms. J Am Chem Soc, 73(1): 373–380

Borysenko A, Clennell B, Sedev R, Burgar I, Ralston J, Raven M, Dewhurst D, Liu K (2009). Experimental investigations of the wettability of clays and shales. J Geophys Res, 114(B7): B07202

Bowker K A (2007). Barnett Shale gas production, Fort Worth Basin: issues and discussion. AAPG Bull, 91(4): 523–533

Chalmers G R L, Bustin R M (2007). The organic matter distribution and methane capacity of the Lower Cretaceous strata of Northeastern British Columbia, Canada. Int J Coal Geol, 70(1–3): 223–239

Chalmers G R L, Bustin R M, Power I M (2012). Characterization of gas shale pore systems by porosimetry, pycnometry, surface area, and field emission scanning electron microscopy/transmission electron microscopy image analyses: examples from the Barnett, Woodford, Haynesville, Marcellus, and Doig units. AAPG Bull, 96(6): 1099–1119

Chen F, Zheng Q, Ding X, Lu S, Zhao H (2020b). Pore size distributions contributed by OM, clay and other minerals in over-mature marine shale: a case study of the Longmaxi shale from Southeast Chongqing, China. Mar Pet Geol, 122: 104679

Chen X, Chen L, Tan X, Jiang S, Wang C (2021). Impact of pyrite on shale gas enrichment—a case study of the Lower Silurian Longmaxi Formation in southeast Sichuan Basin. Front Earth Sci, 15(2): 332–342

Chen Y, Wang Y, Guo M, Wu H, Li J, Wu W, Zhao J (2020a). Differential enrichment mechanism of organic matters in the marine-continental transitional shale in northeastern Ordos Basin, China: control of sedimentary environments. J Nat Gas Sci Eng, 83: 103625

Cheng A, Huang W (2004). Selective adsorption of hydrocarbon gases on clays and organic matter. Org Geochem, 35(4): 413–423

Cheng P, Tian H, Xiao X, Gai H, Li T, Wang X (2017). Water distribution in overmature Organic-Rich shales: implications from water adsorption experiments. Energy Fuels, 31(12): 13120–13132

Cortes J E, Mejía-Molina A, Vargas C A, Cortes S I (2019). High-resolution molecular stratigraphy of Oligocene–Miocene sequence of Tumaco-1-ST-P well, Tumaco forearc Basin, Colombia. J Pet Explor Prod Technol, 9(3): 1747–1800

Curtis J B (2002). Fractured shale-gas systems. AAPG Bull, 86(11): 1921–1938

Deng Z, Liu H, Kang Y (2008). Estimation methods of lost gas in coalbed gas content testing. Nat Gas Ind, 28: 85–86 (in Chinese)

Dong D, Gao S, Huang J, Guan Q, Wang S, Wang Y (2015). Discussion on the exploration & development prospect of shale gas in the Sichuan Basin. Nat Gas Ind B, 2(1): 9–23

Furmann A, Mastalerz M, Bish D L, Schimmelmann A, Pedersen P K (2016). Porosity and pore size distribution in mudrocks from the Belle Fourche and Second White Specks Formations in Alberta, Canada. AAPG Bull, 100(8): 1265–1288

Gasparik M, Bertier P, Gensterblum Y, Ghanizadeh A, Krooss B M, Littke R (2014). Geological controls on the methane storage capacity in organic-rich shales. Int J Coal Geol, 123: 34–51

Ge T, Pan J, Wang K, Liu W, Mou P, Wang X (2020). Heterogeneity of pore structure of late Paleozoic transitional facies coal-bearing shale in the southern North China and its main controlling factors. Mar Pet Geol, 122: 104710

Guo T, Zhang H (2014). Formation and enrichment mode of Jiaoshiba shale gas field, Sichuan Basin. Pet Explor Dev, 41(1): 31–40

Guo X, Hu D, Liu R, Wei X, Wei F (2018). Geological conditions and exploration potential of Permian marine-continent transitional facies shale gas in the Sichuan Basin. Nat Gas Ind, 38(10): 11–18 (in Chinese)

Guo Y, Wang P, Chen X, Fang X (2021). Determination of gas adsorption capacity in organic-rich marine shale: a case study of Wufeng-Lower Longmaxi Shale in the southeast Sichuan Basin. Front Earth Sci, 16(3): 541–556

İnan S, Al Badairy H, İnan T, Al Zahrani A (2018). Formation and occurrence of organic matter-hosted porosity in shales. Int J Coal Geol, 199: 39–51

Jarvie D M, Hill R J, Ruble T E, Pollastro R M (2007). Unconventional shale-gas systems: the Mississippian Barnett Shale of north-central Texas as one model for thermogenic shale-gas assessment. AAPG Bull, 91(4): 475–499

Ji L, Qiu J, Song Z, Xia Y (2014). Impact of internal surface area of pores in clay rocks on their adsorption capacity of methane. Geochimica, 3: 238–244 (in Chinese)

Jia T, Wang M, Zhao J (2020). Physical characters of coal shale reservoirs and potential analysis of Qinshui Basin—an example from Y1 Well Linfen City, Shanxi Province. Sci Tech Eng, 20(06): 2169–2178 (in Chinese)

Kuang L, Dong D, He W, Wen S, Sun S, Li S, Qiu Z, Liao X, Li Y, Wu J, Zhang L, Shi Z, Guo W, Zhang S (2020). Geological characteristics and development potential of transitional shale gas in the east margin of the Ordos Basin, NW China. Pet Explor Dev, 47(3): 471–482

Li D, Fu M, Huang Y, Wu D, Xue R (2021b). The characteristics and main controlling factors for the formation of micropores in shale from the Niutitang Formation, Wenshuicun Section, southwest China. Energies, 14(23): 7858

Li J, Tang S, Zhang S, Li L, Wei J, Xi Z, Sun K (2018a). Characterization of unconventional reservoirs and continuous accumulations of natural gas in the Carboniferous-Permian strata, mid-eastern Qinshui Basin, China. J Nat Gas Sci Eng, 49: 298–316

Li P, Zhang J C, Tang X, Huo Z P, Li Z, Luo K Y, Li Z M (2020a). Assessment of shale gas potential of the lower Permian transitional Shanxi-Taiyuan shales in the southern North China Basin. Aust J Earth Sci, 68(2): 262–284

Li P, Zhang J, Rezaee R, Dang W, Tang X, Nie H, Chen S (2021a). Effect of adsorbed moisture on the pore size distribution of marine-continental transitional shales: insights from lithofacies differences and clay swelling. Appl Clay Sci, 201: 105926

Li W, Li J, Lu S, Chen G, Pang X, Zhang P, He T (2022). Evaluation of gas-in-place content and gas-adsorbed ratio using carbon isotope fractionation model: a case study from Longmaxi shales in Sichuan Basin, China. Int J Coal Geol, 249: 103881

Li Z, Liu D, Ranjith P G, Cai Y, Wang Y (2018b). Geological controls on variable gas concentrations: a case study of the northern Gujiao Block, northwestern Qinshui Basin, China. Mar Pet Geol, 92: 582–596

Li Z, Zhang J, Gong D, Tan J, Liu Y, Wang D, Li P, Tong Z, Niu J (2020b). Gas-bearing property of the Lower Cambrian Niutitang Formation shale and its influencing factors: a case study from the Cengong block, northern Guizhou Province, south China. Mar Pet Geol, 120: 104556

Liang J, Huang W, Wang H, Blum M J, Chen J, Wei X, Yang G (2020a). Organic geochemical and petrophysical characteristics of transitional coal-measure shale gas reservoirs and their relationships with sedimentary environments: a case study from the Carboniferous-Permian Qinshui Basin, China. J Petrol Sci Eng, 184: 106510

Liang M, Wang Z, Zheng G, Greenwell H C, Li H, Zhang L, Feng X, Zhang K (2020b). Occurrence and influence of residual gas released by crush methods on pore structure in Longmaxi shale in Yangtze Plate, southern China. China Geology, 3(4): 545–557

Liu S, Wu C, Li T, Wang H (2018). Multiple geochemical proxies controlling the organic matter accumulation of the marine-continental transitional shale: a case study of the Upper Permian Longtan Formation, western Guizhou, China. J Nat Gas Sci Eng, 56: 152–165

Loucks R G, Reed R M, Ruppel S C, Jarvie D M (2009). Morphology, genesis, and distribution of nanometer-scale pores in siliceous mudstones of the Mississippian Barnett Shale. J Sediment Res, 79(12): 848–861

Luo Q, Xiao Z, Dong C, Ye X, Li H, Zhang Y, Ma Y, Ma L, Xu Y (2019). The geochemical characteristics and gas potential of the Longtan formation in the eastern Sichuan Basin, China. J Petrol Sci Eng, 179: 1102–1113

Ma R, Zhang J, Wang M, Ma W, Zhao J (2021). Micro-pore characteristics and gas-bearing properties of marine continental transitional shale reservoirs in the Qinshui Basin. J Henan Polytechnic U (Nat Sci), 40(04): 66–77 (in Chinese)

Mastalerz M, Schimmelmann A, Drobniak A, Chen Y (2013). Porosity of Devonian and Mississippian New Albany Shale across a maturation gradient: insights from organic petrology, gas

adsorption, and mercury intrusion. AAPG Bull, 97(10): 1621–1643

Merkel A, Fink R, Littke R (2015). The role of pre-adsorbed water on methane sorption capacity of Bossier and Haynesville shales. Int J Coal Geol, 147–148: 1–8

Milliken K L, Olson T M (2017). Silica diagenesis, porosity evolution, and mechanical behavior in siliceous mudstones, mowry shale (Cretaceous), Rocky Mountains, USA J Sediment Res, 87(4): 366–387

Milliken K L, Rudnicki M, Awwiller D N, Zhang T (2013). Organic matter-hosted pore system, Marcellus Formation (Devonian), Pennsylvania. AAPG Bull, 97(2): 177–200

Pan L, Xiao X, Tian H, Zhou Q, Chen J, Li T, Wei Q (2015). A preliminary study on the characterization and controlling factors of porosity and pore structure of the Permian shales in Lower Yangtze region, eastern China. Int J Coal Geol, 146: 68–78

Pecharsky V, Zavalij P (2008). Fundamentals of powder diffraction and structural characterization of materials. Springer Science & Business Media

Peng C, Zou C, Zhou T, Li K, Yang Y, Zhang G, Wang W (2017). Factors affecting coalbed methane (CBM) well productivity in the Shizhuangnan block of southern Qinshui basin, north China: investigation by geophysical log, experiment and production data. Fuel, 191: 427–441

Peng Y, Guo S, Zhai G, Shi D, Chen R (2019). Determination of critical parameters for evaluating coal measure shale gas in China. Mar Pet Geol, 109: 732–739

Pollastro R M (2007). Total petroleum system assessment of undiscovered resources in the giant Barnett Shale continuous (unconventional) gas accumulation, Fort Worth Basin, Texas. AAPG Bull, 91(4): 551–578

Qiao J, Littke R, Zieger L, Jiang Z, Fink R (2020). Controls on gas storage characteristics of Upper Paleozoic shales from the southeastern Ordos Basin. Mar Pet Geol, 117: 104377

Qin J, Fu X, Shen B, Liu W, Teng G, Zhang Q, Jiang Q (2010). Characteristics of ultramicroscopic organic lithology of excellent marine shale in the upper Permian sequence, Sichuan Basin. Petrol Geol Experi, 32(02): 164–170 (in Chinese)

Qiu Z, Song D, Zhang L, Zhang Q, Zhao Q, Wang Y, Liu H, Liu D, Li S, Li X (2021). The geochemical and pore characteristics of a typical marine–continental transitional gas shale: a case study of the Permian Shanxi Formation on the eastern margin of the Ordos Basin. Energy Rep, 7: 3726–3736

Romero-Sarmiento M, Rouzaud J, Bernard S, Deldicque D, Thomas M, Littke R (2014). Evolution of Barnett Shale organic carbon structure and nanostructure with increasing maturation. Org Geochem, 71: 7–16

Ross D J K, Bustin R M (2008). Characterizing the shale gas resource potential of Devonian Mississippian strata in the western Canada sedimentary basin: application of an integrated formation evaluation. AAPG Bull, 92(1): 87–125

Saidian M, Godinez L J, Prasad M (2016). Effect of clay and organic matter on nitrogen adsorption specific surface area and cation exchange capacity in shales (mudrocks). J Nat Gas Sci Eng, 33: 1095–1106

Shao L, Xiao Z, Lu J, He Z, Wang H, Zhang P (2007). Permo-Carboniferous coal measures in the Qinshui Basin: lithofacies paleogeography and its control on coal accumulation. Front Earth Sci China, 1(1): 106–115

Shao L, Yang Z, Fang C, Wang S, Gu J, Zhang W, Lu J (2021). Permo-Carboniferous marine-terrestrial transitional facies coal measures shale gas geological conditions and exploration potential in Qinshui Basin. Coal Geol China, 33(10): 1–10 (in Chinese)

Shi X, Zhou S, Tian C, Li D, Li D, Li Y, Wu W, Cai C (2021). Methane adsorption characteristics and controlling factors of deep shale gas in southern Sichuan Basin. China Nat Gas Geosci, 32(11): 1735–1747 (in Chinese)

Strąpoć D, Mastalerz M, Schimmelmann A, Drobniak A, Hasenmueller N R (2010). Geochemical constraints on the origin and volume of gas in the New Albany Shale (Devonian–Mississippian), eastern Illinois Basin. AAPG Bull, 94(11): 1713–1740

Su Y, Zhang Q, Wei Z (2016). Permo-Carboniferous shale gas resources potential assessment in Qinshui Basin. Coal Geol China, 28(04): 27–34 (in Chinese)

Sun J, Wei Q, Yan B, Xiao X (2018). Desorption process and variation of chemical and carbon isotopic composition of coalbed adsorbed gas based on the results of thermal simulation. J China Coal Soc, 43(10): 2848–2856 (in Chinese)

Sun J, Xiao X, Cheng P (2021). Influence of water on shale pore heterogeneity and the implications for shale gas-bearing property — a case study of marine Longmaxi Formation shale in northern Guizhou. Mar Pet Geol, 134: 105379

Sun J, Xiao X, Wei Q, Cheng P, Tian H, Wu Y (2020a). Gas in place and its controlling factors of the shallow Longmaxi shale in the Xishui area, Guizhou, China. J Nat Gas Sci Eng, 77: 103272

Sun Z, Li X, Liu W, Zhang T, He M, Nasrabadi H (2020b). Molecular dynamics of methane flow behavior through realistic organic nanopores under geologic shale condition: pore size and kerogen types. Chem Eng J, 398: 124341

Tang X, Zhang J, Ding W, Yu B, Wang L, Ma Y, Yang Y, Chen H, Huang H, Zhao P (2016). The reservoir property of the Upper Paleozoic marine-continental transitional shale and its gas-bearing capacity in the southeastern Ordos Basin. Earth Sci Front, 23(02): 147–157 (in Chinese)

Tang X, Zhang T, Zhang J, Sun X, Wu C, Jin Z (2020). Effects of pore fluids on methane sorption in the Lower Bakken Shales, Williston Basin, USA. Fuel, 282: 118457

Teng G, Lu L, Yu L, Zhang W, Pan A, Shen B, Wang Y, Yang Y, Gao Z (2021). Formation, preservation and connectivity control of organic pores in shale. Pet Explor Dev, 48(04): 687–699 (in Chinese)

Tian H, Pan L, Xiao X, Wilkins R W T, Meng Z, Huang B (2013). A preliminary study on the pore characterization of Lower Silurian black shales in the Chuandong Thrust Fold Belt, southwestern China using low pressure N_2 adsorption and FE-SEM methods. Mar Pet Geol, 48: 8–19

Tian H, Pan L, Zhang T, Xiao X, Meng Z, Huang B (2015). Pore characterization of organic-rich Lower Cambrian shales in Qiannan Depression of Guizhou Province, southwestern China. Mar Pet Geol, 62: 28–43

Vandenbroucke M, Largeau C (2007). Kerogen origin, evolution and

structure. Org Geochem, 38(5): 719–833

Wang H, Zhou S, Liu D, Jiao P, Liu H (2020b). Progress and prospect of key experimental technologies for shale gas geological evaluation. Nat Gas Ind, 40(06): 1–17 (in Chinese)

Wang P, Yao S, Jin C, Li X, Zhang K, Liu G, Zang X, Liu S, Jiang Z (2020a). Key reservoir parameter for effective exploration and development of high-over matured marine shales: a case study from the Cambrian Niutitang formation and the Silurian Longmaxi formation, south China. Mar Pet Geol, 121: 104619

Wang S, Song Z, Cao T, Song X (2013). The methane sorption capacity of Paleozoic shales from the Sichuan Basin, China. Mar Pet Geol, 44: 112–119

Wang X, Hou J, Li S, Dou L, Song S, Kang Q, Wang D (2020c). Insight into the nanoscale pore structure of organic-rich shales in the Bakken Formation, USA. J Petrol Sci Eng, 191: 107182

Xi Z, Tang S, Lash G G, Ye Y, Lin D, Zhang B (2021). Depositional controlling factors on pore distribution and structure in the lower Silurian Longmaxi shales: insight from geochemistry and petrology. Mar Pet Geol, 130: 105114

Xi Z, Tang S, Li J, Li L (2017b). Investigation of pore structure and fractal characteristics of marine-continental transitional shale in the east-central of Qinshui Basin. Nat Gas Geosci, 28(03): 366–376 (in Chinese)

Xi Z, Tang S, Wang J, Yang G, Li L (2018). Formation and development of pore structure in marine-continental transitional shale from northern China across a maturation gradient: insights from gas adsorption and mercury intrusion. Int J Coal Geol, 200: 87–102

Xi Z, Tang S, Zhang S, Sun K (2017a). Pore structure characteristics of marine–continental transitional shale: a case study in the Qinshui Basin, China. Energy Fuels, 31(8): 7854–7866

Xie W, Wang M, Wang H, Ma R, Duan H (2021). Diagenesis of shale and its control on pore structure, a case study from typical marine, transitional and continental shales. Front Earth Sci, 15(2): 378–394

Xu H, Pan Z, Hu B, Liu H, Sun G (2020a). A new approach to estimating coal gas content for deep core sample. Fuel, 277: 118246

Xu S, Hao F, Shu Z, Zhang A, Yang F (2020b). Pore structures of different types of shales and shale gas exploration of the Ordovician Wufeng and Silurian Longmaxi successions in the eastern Sichuan Basin, south China. J Asian Earth Sci, 193: 104271

Yang C, Xiong Y, Zhang J, Liu Y, Chen C (2019). Comprehensive understanding of OM-Hosted pores in transitional shale: a case study of Permian Longtan Shale in south China based on organic petrographic analysis, gas adsorption, and X-ray diffraction measurements. Energy Fuels, 33(9): 8055–8064

Yang C, Zhang J, Tang X, Ding J, Zhao Q, Dang W, Chen H, Su Y, Li B, Lu D (2017). Comparative study on micro-pore structure of marine, terrestrial, and transitional shales in key areas, China. Int J Coal Geol, 171: 76–92

Yin L, Guo S (2019). Full-sized pore structure and fractal characteristics of marine-continental transitional shale: a case study in Qinshui Basin, north China. Acta Geol Sin (English Edition), 93(3): 675–691

Yu K, Ju Y, Zhang B (2020). Modeling of tectono-thermal evolution of Permo-Carboniferous source rocks in the southern Qinshui Basin, China: consequences for hydrocarbon generation. J Petrol Sci Eng, 193: 107343

Yuan Y, Rezaee R, Yu H, Zou J, Liu K, Zhang Y (2021). Compositional controls on nanopore structure in different shale lithofacies: a comparison with pure clays and isolated kerogens. Fuel, 303: 121079

Zhang J, Fan T, Li J, Zhang J, Li Y, Wu Y, Xiong W (2015). Characterization of the lower cambrian shale in the northwestern Guizhou Province, south China: implications for shale-gas potential. Energy Fuels, 29(10): 6383–6393

Zhang J, Li X, Wei Q, Sun K, Zhang G, Wang F (2017a). Characterization of full-sized pore structure and fractal characteristics of marine–continental transitional Longtan Formation Shale of Sichuan Basin, south China. Energy Fuels, 31(10): 10490–10504

Zhang J, Li X, Xiaoyan Z, Zhao G, Zhou B, Li J, Xie Z, Wang F (2019a). Characterization of the Full-Sized pore structure of coal-bearing shales and its effect on shale gas content. Energy Fuels, 33(3): 1969–1982

Zhang J, Li X, Zhang X, Zhang M, Cong G, Zhang G, Wang F (2018). Geochemical and geological characterization of marine–continental transitional shales from Longtan Formation in Yangtze area, south China. Mar Pet Geol, 96: 1–15

Zhang J, Liu D, Cai Y, Pan Z, Yao Y, Wang Y (2017b). Geological and hydrological controls on the accumulation of coalbed methane within the No. 3 coal seam of the southern Qinshui Basin. Int J Coal Geol, 182: 94–111

Zhang L, Dong D, Qiu Z, Wu C, Zhang Q, Wang Y, Liu D, Deng Z, Zhou S, Pan S (2021). Sedimentology and geochemistry of Carboniferous-Permian marine-continental transitional shales in the eastern Ordos Basin, north China. Palaeogeogr Palaeoclimatol Palaeoecol, 571: 110389

Zhang M, Fu X (2018). Study of the characteristics of marine-terrigenous facies shale from the Permo-Carboniferous system in the Guxian Block, southwest Qinshui Basin. Energy Fuels, 32(2): 1096–1109

Zhang M, Fu X (2019). Influence of reservoir properties on the adsorption capacity and fractal features of shales from Qinshui coalfield. J Petrol Sci Eng, 177: 650–662

Zhang M, Fu X, Zhang Q, Cheng W (2019b). Research on the organic geochemical and mineral composition properties and its influence on pore structure of coal-measure shales in Yushe-Wuxiang Block, South Central Qinshui Basin, China. J Petrol Sci Eng, 173: 1065–1079

Zhang Q, Liu H, Bai W, Lin W (2013). Shale gas content and its main controlling factors in Longmaxi shale in southeastern Chongqing. Nat Gas Ind, 33(05): 35–39 (in Chinese)

Zhang T, Ellis G S, Ruppel S C, Milliken K L, Yang R (2012). Effect of organic-matter type and thermal maturity on methane adsorption in shale-gas systems. Org Geochem, 47: 120–131

Zhang X, Li X, Li Y, He Y, Zhang J, Zhang Y (2020). Research progress of reservoir of shale gas in coal measures. Coal Geol China, 32(02): 59–66 (in Chinese)

Zhao J, Fu X, Zhang M, Cheng W, Qu L (2019). Evaluation of organic geochemical characteristics and hydrocarbon generation potential of

coal measure mud shale. Coal Sci Technol, 47(11): 182–188 (in Chinese)

Zhao J, Jin Z, Hu Q, Liu K, Jin Z, Hu Z, Nie H, Du W, Yan C, Wang R (2018). Mineral composition and seal condition implicated in pore structure development of organic-rich Longmaxi shales, Sichuan Basin, China. Mar Pet Geol, 98: 507–522

Zhao W, Jia A, Wei Y, Wang J, Zhu H (2020). Progress in shale gas exploration in China and prospects for future development. China Petrol Explor, 25(1): 31–44 (in Chinese)

Zhao W, Li J, Yang T, Wang S, Huang J (2016). Geological difference and its significance of marine shale gases in south China. Pet Explor Dev, 43(4): 547–559

Zheng X, Zhang B, Sanei H, Bao H, Meng Z, Wang C, Li K (2019). Pore structure characteristics and its effect on shale gas adsorption and desorption behavior. Mar Pet Geol, 100: 165–178

Zhong Q, Fu X, Zhang M, Zhang Q, Cheng B (2020). Development potential of Carboniferous—Permian coal measures shale gas in Qinshui coalfield. Nat Gas Geosci, 31(01): 110–121 (in Chinese)

Zhou S (2002). Coalbed gas content simulation test and application. Coal Geol Explor, 30: 25–28 (in Chinese)

Zhu S, Salmachi A (2021). Flowing material balance and rate-transient analysis of horizontal wells in under-saturated coal seam gas reservoirs: a case study from the Qinshui Basin, China. Energies, 14(16): 4887

Zou Z, Liu D, Cai Y, Wang Y, Li J (2018). Geological factors and reservoir properties affecting the gas content of coal seams in the Gujiao area, northwest Qinshui Basin, China. Energies, 11(5): 1044